



Microporous separators for Fe/V redox flow batteries

Xiaoliang Wei^a, Liyu Li^b, Qingtao Luo^a, Zimin Nie^a, Wei Wang^{a,*}, Bin Li^a, Guan-Guang Xia^a, Eric Miller^c, Jeff Chambers^c, Zhenguo Yang^b

^a Pacific Northwest National Laboratory, 902 Battelle Blvd, PO BOX 999, Richland, WA 99354, USA

^b UniEnergy Technologies, LLC, 4333 Harbour Pointe Blvd SW, Unit A, Mukilteo, WA 98275, USA

^c Daramic LLC, 5525 US 60 East, Owensboro, KY 42303, USA

HIGHLIGHTS

- Inexpensive microporous separators were successfully utilized on Fe/V RFB.
- Capacity fading during cycling was alleviated with flow rate adjustment.
- Cycling performances at different temperatures were investigated.

ARTICLE INFO

Article history:

Received 21 May 2012

Received in revised form

20 June 2012

Accepted 21 June 2012

Available online 28 June 2012

Keywords:

Iron–vanadium

Microporous separator

Hydraulic pressure

Electrolyte

Redox flow battery

ABSTRACT

The Fe/V redox flow battery has demonstrated promising performance with distinct advantages over other redox flow battery systems. Due to the less oxidative nature of the Fe(III) species, hydrocarbon-based ion exchange membranes or separators can be used. Daramic® microporous polyethylene separators were tested on Fe/V flow cells using sulphuric/chloric mixed acid-supporting electrolytes. Among them, separator C exhibited good flow cell cycling performance with satisfactory repeatability over a broad temperature range of 5–50 °C. Energy efficiency (EE) of C remains around 70% at current densities of 50–80 mA cm⁻² in temperatures ranging from room temperature to 50 °C. The capacity decay problem could be circumvented through hydraulic pressure balancing by means of applying different pump rates to the positive and negative electrolytes. Stable capacity and energy were obtained over 20 cycles at room temperature and 40 °C. These results show that extremely low-cost separators (\$1–20 m⁻²) are applicable in the Fe/V flow battery system with acceptable energy efficiency. This represents a remarkable breakthrough: a significant reduction of the capital cost of the Fe/V flow battery system, which could further its market penetration in grid stabilization and renewable integration.

© 2012 Elsevier B.V. All rights reserved.

1. Introduction

Energy storage systems are of great interest for their capacity to balance the discrepancy between energy generation and consumption. Recently, redox flow batteries (RFBs), which are capable of reversibly converting between electrical and chemical energies, have experienced revitalization as a promising large-scale energy storage technique [1,2]. RFBs enable reliable integration of intermittent renewable energy resources such as solar [3] or wind [4], functioning as an energy reservoir to improve power output quality. An important advantage of RFBs is their decoupled power and energy. The power is controlled by the size of the electrodes, while the energy is dependent on the concentration and volume of

the electrolytes contained in external tanks. RFBs have many other attractive features such as: high round-trip efficiency, long cycle durability and calendar life, rapid response to load changes, and active thermal management [5].

Development of practical RFBs started from the iron–chromium RFB invented by Thaller [6], while the invention of an all-vanadium flow battery (VRB) by Sylitas-Kazacos [7–10] is another significant breakthrough. Despite impressive advantages, the drawbacks of VRB are also obvious, limiting its broad market penetration. One of the disadvantages with VRBs is the membrane chemical stability issue. As one key component, the membrane physically separates the positive and negative electrolytes yet allows passage of charge carriers to maintain electrical neutrality. In VRBs, the membrane must be chemically stable to the strongly oxidative V(V) species. This requirement largely narrows the membrane choice to per-fluorinated Nafion®-based ion exchange membranes (Nafion® is a registered trademark of DuPont). However, these membranes are

* Corresponding author. Tel.: +1 509 372 4097; fax: +1 509 375 2186.

E-mail address: wei.wang@pnnl.gov (W. Wang).

quite expensive, accounting for 41% of the flow battery stack cost based on a cost analysis [11]. Hydrocarbon-based membranes are being studied [12], but their long-term chemical stability remains a concern. Capacity decay is another challenge for VRB systems [13–15], which requires frequent maintenance by mixing the electrolytes [16] and increases operational costs.

The recent invention of an iron–vanadium (Fe/V) flow battery system uses mixed Fe/V electrolytes with $\text{Fe}^{2+}/\text{Fe}^{3+}$ and $\text{V}^{3+}/\text{V}^{4+}$ as positive and negative redox couples [17,18]. The Fe/V flow battery has a standard voltage of 1.02 V with the standard redox potentials of $\text{Fe}^{2+}/\text{Fe}^{3+}$ and $\text{V}^{3+}/\text{V}^{4+}$ at 0.77 V and –0.25 V (versus standard hydrogen electrode, SHE), respectively. This mitigates the gas evolution that remains an issue for VRBs. At room temperature, the Fe/V flow battery exhibits columbic (CE), voltage (VE), and energy efficiencies (EE) as high as 97%, 85%, and 82%, respectively, at a current density of 50 mA cm^{-2} when using a Nafion 212 membrane. Stable performance was achieved over a temperature range of 0–50 °C. The Fe/V flow battery shows excellent capability to retain its capacity and energy, and the maintenance costs will be significantly reduced. Therefore, the Fe/V flow battery is particularly advantageous for renewable integration and stabilization of the electrical grid.

Due to the lower cell voltage, the discharge energy density of the Fe/V flow battery (up to 15 Wh L^{-1}) usually is lower than that of the recent invented mixed-acid VRB [19]. Yet, it is on par with the conventional VRB sulphate system. Therefore, reducing the capital cost of the Fe/V system is necessary to make it competitive with the VRB. The less oxidative nature of Fe^{3+} enables the use of inexpensive hydrocarbon-based membranes or separators. Daramic® (a registered trademark of Daramic, LLC.) microporous polyethylene separators lead the flooded lead acid battery market due to their low cost ($\$1–20 \text{ m}^{-2}$), low electrical resistance, excellent microporous structure, designable pore size, and porosity [20]. Daramic® separators have been attempted in VRB applications, but they are susceptible to chemical attack of the V(V) species [21–27]. This paper explores applications of Daramic® separators in the Fe/V flow battery. The flow cell performance of a series of commercial Daramic® microporous separators on the Fe/V flow battery was investigated. The dependence of CE, VE, and EE on separator resistance will be discussed, and the effects of temperature and current density will be presented.

2. Experimental

2.1. Fe/V flow cell setup

The Fe/V flow cell assembly followed that used in Ref. [13]. Typically, the flow cell consisted of two stainless-steel end plates; two gold-coated copper current collectors; two graphite half-cell compartments, each with a rectangular trough as well as an inlet and an outlet; two 5 mm-thick graphite felt electrodes (GFD5, SGL Carbon Group, Germany); two polytetrafluoroethylene (PTFE) gaskets; and a separator. The felts embedded in the troughs had a 10% compression ratio to afford optimal electrical conductivity. The active areas of the GFD5 and the Daramic® separator were $5 \text{ cm} \times 2 \text{ cm}$. Thermal activation of the GFD5 was carried out in air at 400 °C for 6 h to enhance its electrochemical activity and wettability [28]. Viton® tubing (Cole–Parmer, Vernon Hills, IL) was piped through a Masterflex® L/S® peristaltic pump (Cole–Parmer, Vernon Hills, IL) equipped with an Easy-Load® II pump head (Cole–Parmer, Vernon Hills, IL) and connected the flow cell with two glass beaker reservoirs.

2.2. Electrochemical measurement

Five Daramic® microporous separators named A, B, C, D, and E were supplied by Daramic, LLC (Charlotte, NC). These separators

differ in terms of thickness and structure. Among them, D and E have parallel ribs protruding from one side of the separator. The ribs were mechanically removed prior to pre-treatment. All separators were pre-treated by alternative methanol and deionized water soakings.

The electrolyte was prepared by dissolving vanadyl sulphate (VOSO_4 , Sigma–Aldrich, 99%) and iron(II) chloride (FeCl_2 , Sigma–Aldrich, 98%) in diluted HCl. The final concentration of the electrolyte is: 1.5 M VOSO_4 –1.5 M FeCl_2 –3.6 M HCl (hereafter abbreviated as 1.5Fe/V–3.6HCl). Unless otherwise stated, 50 mL of the electrolyte was used in each of the positive and negative reservoirs of the balanced flow cell. To keep the system oxygen-free, both reservoirs were purged with nitrogen before each cell run. The electrical impedance of the flow cell was measured by alternative current impedance spectroscopy (ACIS) on a CHI760D electrochemical workstation (CH Instruments, Austin, TX) at a flow rate of 20 mL min^{-1} . The area-specific resistivity (ASR) of the flow cell was derived by the high-frequency resistance (the real part of the ACIS) multiplied by the cell area (10 cm^2). A BT-2000 Arbin battery tester (Arbin Instruments, College Station, TX) was used to evaluate the cell performance under constant current mode. The charge–discharge voltage window was set between 1.35 V and 0.5 V for flow cell cycling. Different current densities, such as 40, 50, 60, 70, and 80 mA cm^{-2} , were used to investigate current density effect. The temperature effect was examined by running the flow cell in a Tenney TJR junior benchtop chamber (Thermal Product Solutions, White Deer, PA). The concentrations of the Fe and V species in the electrolytes after cycling were determined by an Optima 7300 DV inductively coupled plasma (ICP) (PerkinElmer, Waltham, MA).

3. Results and discussion

3.1. Room temperature cell performance

Typical parameters of these Daramic® polyethylene microporous separators include median pore size of $0.15 \mu\text{m}$ with porosity of 57%. The thickness ranges from 200 to $500 \mu\text{m}$. A cross-sectional scanning electron microscopy (SEM) image is also provided in the Supplemental Information (Figure S1) indicating silica particles embedded in polyethylene matrix. The Fe/V flow cell performance of these separators was tested at room temperature (18 °C) using the sulphuric/chloric mixed acid-supporting electrolyte, 1.5Fe/V–3.6HCl, with a voltage range of 0.5–1.2 V at a current density of 50 mA cm^{-2} . To lower the separators' resistance, they were pre-treated by alternative methanol and water immersions prior to each use to remove air bubbles trapped inside the pores. The pre-treatment was followed by swift assembly of the flow cell.

The flow cell resistance obtained using ACIS includes the resistances of the separator and the electrolyte, and the contact resistance. While the latter two are independent of the separator and remain constant for all the cells tested, the flow cell ASR indicates the relative resistance of these separators. In this sense, flow cell ASR is determined by the thickness and structure of the separators. Fig. 1a shows the influence of ASR on flow cell cycling efficiencies [29]. Constant efficiencies were observed throughout the Fe/V flow cell cycling, indicating good stability of the separator [30,31]. The CE, VE, and EE of these separators are closely related to flow cell ASR. The CE increases gradually with the ASR, while the VE exhibits a negative linear correlation with the ASR. Separator A has the lowest flow cell ASR of $0.66 \Omega \text{ cm}^2$, therefore the lowest CE of 82% and highest VE of 84%. On the contrary, separator B has the highest flow cell ASR of $2.32 \Omega \text{ cm}^2$, thus the highest CE of 95% and lowest VE of 67%. Among these separators, A, C, D, and E afford EEs around 70%. Separators A, C, D, and E, which offered the highest EEs, were

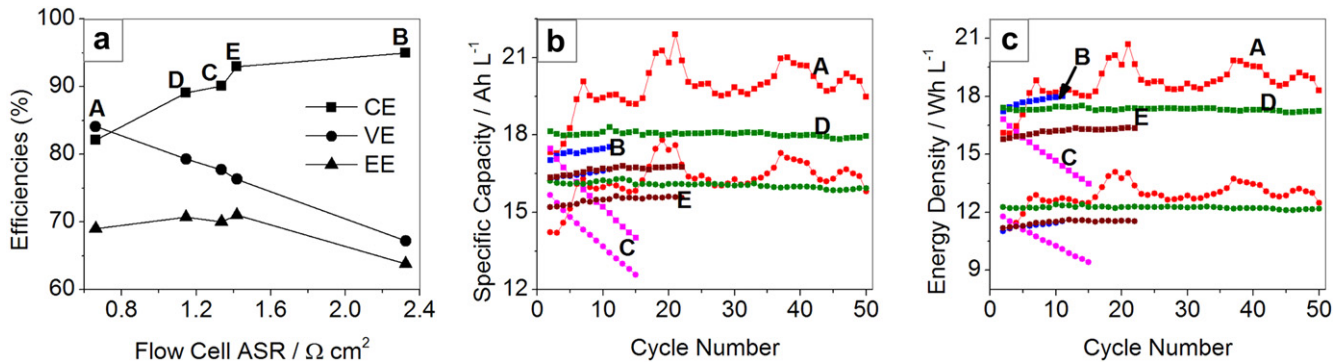


Fig. 1. Room temperature Fe/V flow cell performance of Daramic® separators at a current density of 50 mA cm^{-2} : (a) flow cell efficiencies versus flow cell ASR; (b) specific capacity; and (c) energy density versus cycle number of different separators.

considered for further study of temperature and current density effects.

In general, the CE, VE, and EE of flow cells with separators are lower than those with Nafion 212 membrane [17,18]. The separators have a different ion transport mechanism from that of the ion exchange membranes [32]. The inter-connected micro-pores provide much larger channels for charge carrier transport. The Fe or V species encounter smaller barriers to cross-separator transport, which yields a lower CE. The selectivity of protons over the Fe or V species possibly originates from the higher transport rate of the smaller protons than that of the larger Fe or V species driven by the concentration and potential gradients. A similar phenomenon was reported for nanofiltration membranes tested in a VRB system [33,34]. The reason for the lower VE is the higher ohmic resistance of the separators in that: 1) they lack a proton surface hopping mechanism and 2) are significantly thicker than Nafion 212 (50 μm).

Fig. 1b shows the specific charge and discharge capacities with respect to the cycle number for the separators, while Fig. 1c depicts the charge and discharge energy densities. On the whole, the cycling performance of separator A was stable, although noticeable oscillations existed. The mechanism of the oscillations is not yet well understood and is hypothesized to be related with unstable cross transport of the Fe or V active species. Separators B, D, and E exhibit excellent capacity and energy retention capability similar to that of the previously reported cycling performance from the Nafion 212 flow cell [17,18]. Especially, separator D exhibits a stable performance over 50 cycles. The positive and negative electrolytes maintained a constant volume (50 mL) during cycling with no observable volume change, indicating negligible water transfer between positive and negative half-cells. The capacity and energy of separator C demonstrated constant decay at a rate of $\sim 2\%$ per cycle, although its CE, VE, and EE remain constant. A noticeable electrolyte volume change was observed along the cycling, indicating water transfer from the positive to the negative side [35].

3.2. The temperature effect

Temperature stability is an important variable to evaluate an RFB system in practical use, and the operational temperature range must be determined in terms of stability and efficiency. This is particularly critical for RBFs built at remote places with no active thermal management systems. For example, the active thermal management system attached to a conventional VRB sulphate system must maintain the temperature between 0 and 40 °C to prevent precipitation of the active species [36]. A Fe/V flow battery using a Nafion 212 membrane with sulphuric/chloric mixed acid-supporting electrolytes was able to operate between 0 and 50 °C

while maintaining stable performance with EE spanning 67–80% at a current density of 50 mA cm^{-2} [18].

Temperature induces changes to both CE and VE. Elevated temperature increases both the crossover transport of the active species across the separator and the electrical conductivity of the electrolyte, yielding a lower CE and higher VE. The former may cause unbalanced water and ion cross transports that result in attenuated capacity retention capability. Fig. 2a displays the specific charge capacity and discharge energy density of separators A, C, D, and E at 40 °C at a current density of 50 mA cm^{-2} . Interestingly, despite the existence of slight oscillations, separator D still retained the capacity and energy during cycling. However, separators A, C, and E underwent fast capacity drops at a rate of 3.6%, 3.9%, and 1.4%, respectively. Therefore, increasing temperature accelerates the crossover transport of both water and the active species. Electrolyte volumes changed more rapidly than at room temperature. The capacity and energy decay originates from an unbalanced transfer of the active species across the separator, e.g., net transfers of both Fe and V from the positive to the negative side, which is confirmed by the ICP results as shown in the Supplemental Information (Table S1).

Fig. 2b–d plots the Fe/V flow cell CE, VE, and EE of separators A, C, D, and E at different temperatures of 0, 18, 30, 40, and 50 °C at a current density of 50 mA cm^{-2} . All of the separators demonstrated a similar tendency of decreasing CE and increasing VE with temperature. As the mathematical product of CE and VE, EE depends on how much CE and VE were changed. Separator A exhibited a sharp drop from 69% at room temperature to 62% at 40 °C. From 5 °C to 50 °C, EE of the other three separators experienced a sharp increase before a peak value was reached, followed by drops that were faster at elevated temperatures. Separator C showed a peak EE value of 73.5% at room temperature with 64.7% at 5 °C and 66.6% at 50 °C. Notably, the EE of separator C underwent little change between 73.5% and 71% in the range from room temperature to 40 °C. The very low EE at 5 °C is closely related to the significantly reduced conductivity of the electrolytes at low temperature. Separator D shows a similar phenomenon with an EE of 70.6% at room temperature, 66.2% at 5 °C, and 66.4% at 50 °C. The peak EE value of separator E, 72.4%, appeared at 40 °C, and the temperature range for stable EEs is 18–50 °C.

3.3. The current density effect

For a specified voltage window, current density has a direct impact on the power density delivered by an RFB system. Improved current density can augment the power density, reduce the stack size, and lower the capital cost in an RFB system. Increase of the current density produces a higher overpotential that lowers the VE,

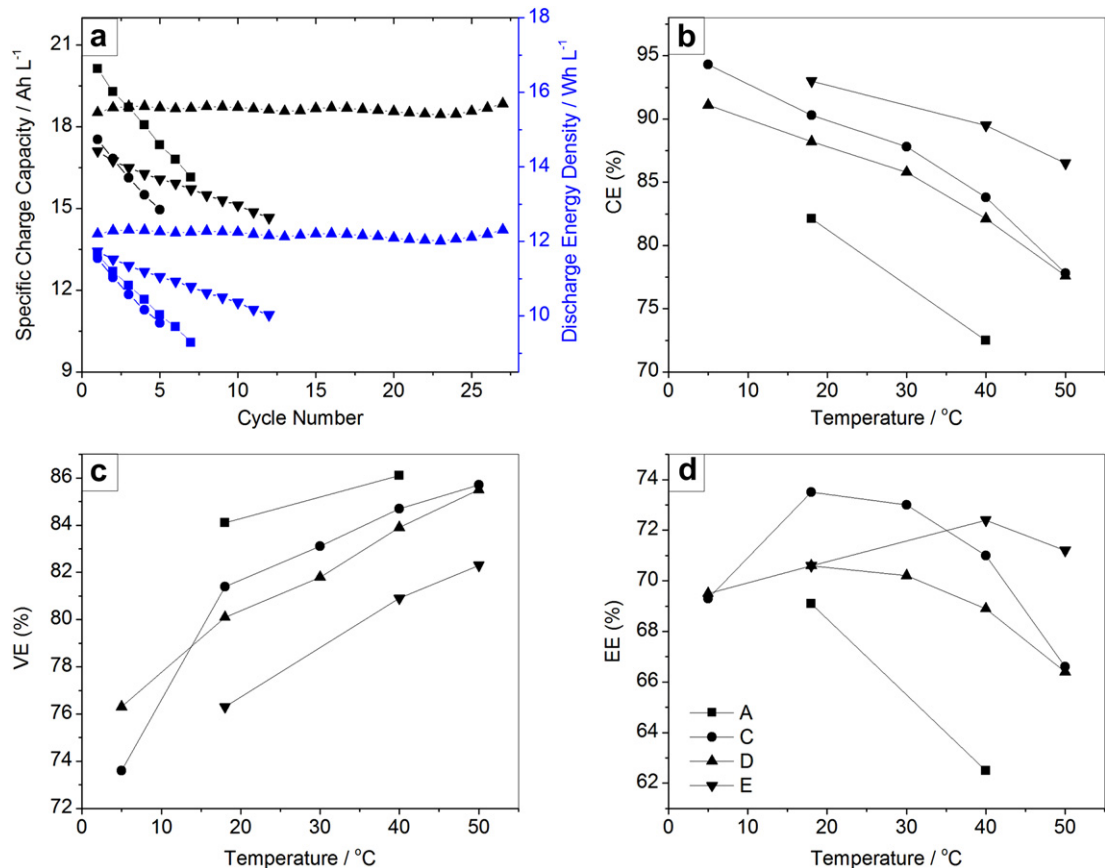


Fig. 2. The temperature effect on cell performance of the separators: (a) specific charge capacity and discharge energy density; (b) CE; (c) VE; and (d) EE of separator A (■), C (●), D (▲), and E (▼).

and mitigates cross transport of the active species that increases the CE.

The performance of the Fe/V flow cell with the separators was studied at different current densities to determine the optimal current density range. Fig. 3 illustrates the cell efficiencies of separator C at current densities of 40, 50, 60, 70, and 80 mA cm⁻² and different temperatures. CE grows with the current density. Temperature appears to have an evident influence in that CE grows faster at higher temperatures. VE reveals a linear decline against the current density under all of the tested temperatures. As a result, EE shows drastically different temperature-dependent behaviours with respect to the current density. The

tendency of EE changes from a rapid decrease at 5 °C to a gradual increase at 50 °C. Strikingly, at room temperature and above, the EE of separator C remains no less than 67% in a current density range of 50–80 mA cm⁻². This indicates that a Fe/V flow battery equipped with separator C has the potential to operate at a current density up to 80 mA cm⁻² and consequently produces an enhanced power output and reduced capital cost. A complete list of the Fe/V flow cell efficiencies at different temperatures and current densities is summarized in the Supplementary Information (Table S2). Separators D and E also show a similar temperature-dependent tendency as a function of the current density.

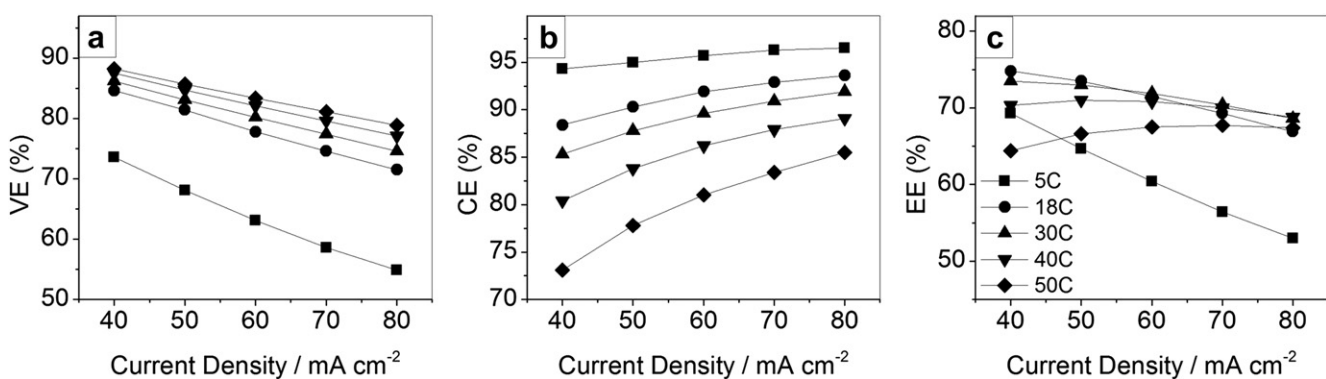


Fig. 3. CE, VE, and EE of separator C as a function of current density in the temperature range of 5–50 °C.

Therefore, separators C, D, and E have demonstrated desirable cell performance over considerably broad ranges of temperature and current density. However, D and E suffer from poor repeatability resulting from the rib cutting that might generate a variable of case-dependent surface pore structure. On the contrary, free from mechanical processing, separator C has shown satisfactory repeatability. Separator C's rapid capacity decay problem can be circumvented by balancing the hydraulic pressure across the separator via adjusting the electrolyte flow rates.

3.4. Hydraulic pressure balancing

Hydraulic pressure has long been applied in membrane processes for water purification, such as microfiltration, ultrafiltration, nanofiltration, and reverse osmosis, as the driving force to counteract osmosis pressure [37]. Similarly, in flow battery systems, it is conceivable to attenuate the unbalanced transport of water and active species by applying counter-hydraulic pressure to the recipient electrolyte [38]. The higher hydraulic pressure impels the water and active species to transport to the opposite direction until equilibrium is reached. In this work, the separators' capacity decay problem was addressed by adopting different flow rates at the positive and negative electrolytes to balance the hydraulic pressure across the separator minimizing the volume change during cycling.

Fig. 4 displays such an attempt using separator D at room temperature at a current density of 50 mA cm^{-2} , with the specific charge capacity and discharge energy density (a) and the efficiencies (b). Table S3 in the Supplementary Information area summarizes the detailed flow rate adjustments during the cell run. This flow cell used 55 mL of the electrolyte in each reservoir and had an ASR of $1.017 \Omega \text{ cm}^2$. In contrast to a previous one with stable capacity, separator D in this case suffered from a low initial capacity followed by rapid capacity decay (8.5% per cycle) until the 14th cycle. The initial efficiencies were CE = 84.1%, VE = 80.4%, and EE = 67.6%. The significantly lower CE of this separator D than the previous one (88.2%) indicates a higher crossover transport of active materials and accounts for the rapid capacity decay. The flow rate adjustment is divided into two zones, depending if high or low pump rates were used. The high pump rate zone was from the 1st to 82nd cycle, and a low pump rate zone was from the 83rd to 169th cycle (shown in Fig. 4). Employing pump rates of 35 mL min^{-1} at the negative side and 15 mL min^{-1} at the positive side caused negative-to-positive transport of water and active species, consequently, a sharp capacity increase from the 15th to 25th cycle. A series of fine-tuning of the pump rates were performed to finally reach equilibrium in the high pump rate zone with pump rates of

26 mL min^{-1} at the negative side and 15 mL min^{-1} at the positive side. The stable specific charge capacity is 18.2 Ah L^{-1} , and discharge energy density is 12.5 Wh L^{-1} . The CE, VE, and EE are 86.7%, 81.5%, and 70.7%, respectively. Interestingly, the efficiencies show changes corresponding to the pump rate adjustment, and the extent of such changes depends on the transport status. For example, in the initial six cycles, the rapid positive-to-negative transport of water and active species was accompanied by an evident rise of CE and drop in VE. The forced positive-to-negative transport in the 15th–26th cycles coexisted with a sharp drop of CE and clear rise of VE. Smaller changes of CE and VE were observed in the other cycles having milder transports.

Low flow rate is preferred in a flow battery stack in order to save the pump energy, which makes it necessary to study the cell cycling and hydraulic balance at low pump rates. A sudden change of the pump rates to 5 mL min^{-1} at positive and 9 mL min^{-1} at negative broke the equilibrium and produced capacity decay. EE underwent a 1.3% drop, resulting from a 1% rise of CE and a 2.7% drop of VE due to the increased mass transfer barrier. Similarly, after a series of fine-tuning the pump rates, equilibrium was reached again at the 126th cycle with a positive pump rate of 5 mL min^{-1} and a negative pump rate of $10/11 \text{ mL min}^{-1}$. Stable performance was maintained over more than 40 cycles with the specific charge capacity and discharge energy density of 17.2 Ah L^{-1} and 11.6 Wh L^{-1} . The CE, VE, and EE are 86.9%, 78.9%, and 68.6%, respectively. This confirms that the long-term stable cycling can be obtained with Fe/V flow battery equipped with separator as the membrane even at low flow rate, which is promising for stack and system development.

Performance stabilization via a similar electrolyte flow rate adjustment method was performed to separator C at low pump rates. Fig. 5a shows the specific charge capacity and discharge energy density of separator C with respect to the cycle number at room temperature. Table S4 in the Supplementary Information summarizes the detailed flow rate adjustment procedure. At room temperature, stable performance was obtained over the course of approximately 20 cycles with the flow rates of 5 mL min^{-1} at the positive side and 20 mL min^{-1} at the negative side. The stable specific charge capacity is 18.8 Ah L^{-1} , and the discharge energy density is 12.9 Wh L^{-1} . The CE, VE, and EE are 90.4%, 77.3%, and 69.9%, respectively. At elevated temperature, additional counter-hydraulic pressure, i.e., a higher flow rate, needs to be applied at the recipient electrolyte (the negative side) to counteract accelerated cross transport of the active species. This room temperature flow cell was moved to a 40°C thermal chamber, and similar flow rate optimization was performed to achieve stable capacity. The specific charge capacity and discharge energy density are shown in

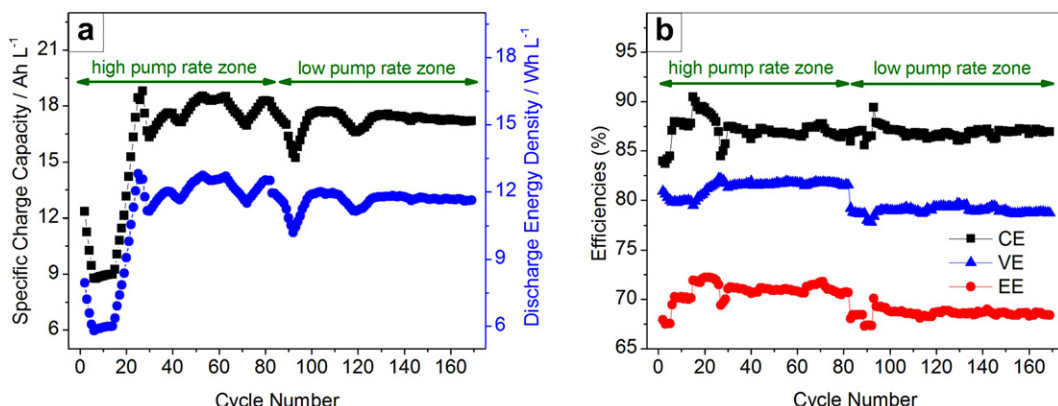


Fig. 4. Performance stabilization through flow rate adjustment for separator D: (a) specific charge capacity and discharge energy density versus cycle number; and (b) CE, VE, and EE.

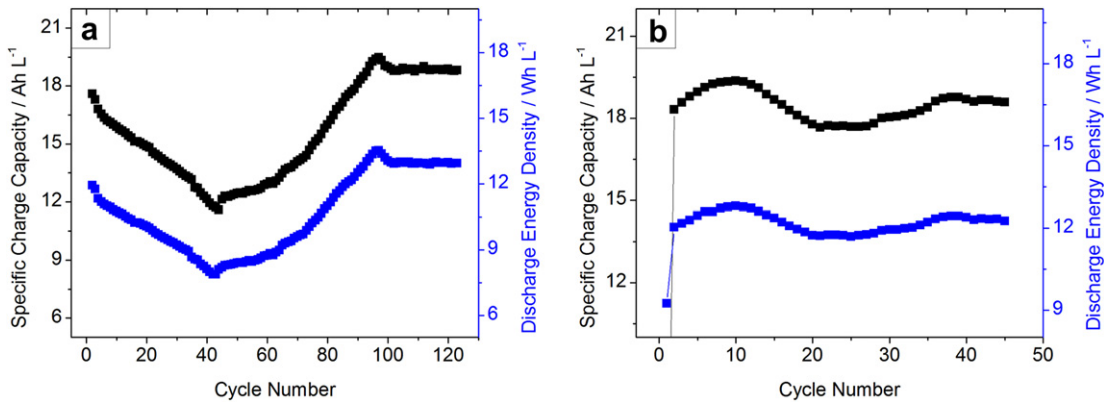


Fig. 5. Performance stabilization for separator C: (a) at room temperature and (b) at 40 °C.

Fig. 5b, and the detailed flow rate adjustment procedure is depicted in Table S4. At 40 °C, stable performance was obtained for up to 40 cycles with the flow rates of 5 mL min⁻¹ at the positive side and 45 mL min⁻¹ at the negative side. The stable specific charge capacity is 18.6 Ah L⁻¹, and the discharge energy density is 12.3 Wh L⁻¹. The CE, VE, and EE are 83.2%, 82.9%, and 69.0%, respectively. The ability to re-establish stable cycling through the simple flow rate adjustment after temperature fluctuation renders the Fe/V system critical operation latitude in maintaining stable cycling during practical use in an environment that will inevitably encounter the climate change.

4. Conclusions

Several Daramic® microporous separators have been tested on Fe/V flow cells using sulphuric/chloric mixed acid-supporting electrolytes. The effects of temperature and current density on flow cell cycling performance were investigated in detail. Among them, separators D and E have desired flow cell performance, but repeatability is poor due to the necessity of rib cutting. Separator C demonstrates attractive cell performance with satisfactory repeatability. Separator C exhibits EEs above 67% at current densities of 50–80 mA cm⁻² in the temperature range of 18–50 °C. Optimization of the hydraulic balance across the separator by applying different flow rates to the positive and negative electrolytes has succeeded in overcoming the rapid capacity decay problem. Stable cell performance (capacity and energy) of separator C has been accomplished over approximately 20 cycles, both at room temperature and at 40 °C. In these cases, the specific charge capacity and discharge energy density could reach 18.8 Ah L⁻¹ and 12.9 Wh L⁻¹ at room temperature and 18.6 Ah L⁻¹ and 12.3 Wh L⁻¹ at 40 °C, respectively.

The ability to use hydrocarbon-based membranes or separators is a compelling advantage of Fe/V over VRB systems. In general, these microporous separators afford relatively inferior cell performance compared to Nafion® membranes. However, considering their availability at nearly 100 times lower cost, the Daramic® separators are a promising replacement for expensive Nafion® membranes with a reasonable sacrifice of EE (less than 10%). Significant reduction in capital cost is expected to enhance the competitiveness of the Fe/V flow cell as an energy storage technology for renewable energy resources integration.

Acknowledgements

The authors would like to acknowledge financial support from the U.S. Department of Energy's (DOE's) Office of Electricity Delivery &

Energy Reliability (OE) (under Contract No. 57558). We are also grateful for useful discussions with Dr. Imre Gyuk of the DOE-OE Grid Storage Program. PNNL is a multi-program national laboratory operated by Battelle for DOE under Contract DE-AC05-76RL01830.

Appendix A. Supplementary material

Supplementary material associated with this article can be found, in the online version, at <http://dx.doi.org/10.1016/j.jpowsour.2012.06.073>.

References

- [1] Z.G. Yang, J.L. Zhang, M.C.W. Kintner-Meyer, X.C. Lu, D.W. Choi, J.P. Lemmon, J. Liu, *Chem. Rev.* 111 (2011) 3577–3613.
- [2] A.Z. Weber, M.M. Mench, J.P. Meyers, P.N. Ross, J.T. Gostick, Q.H. Liu, *J. Appl. Electrochem.* 41 (2011) 1137–1164.
- [3] L. Joerissen, J. Garche, C. Fabjan, G. Tomazic, *J. Power Sources* 127 (2004) 98–104.
- [4] D.C. Holzman, *Environ. Health Perspect.* 115 (2007) A358–A361.
- [5] C.P. de Leon, A. Frias-Ferrer, J. Gonzalez-Garcia, D.A. Szanto, F.C. Walsh, *J. Power Sources* 160 (2006) 716–732.
- [6] L.H. Thaller, in: US Patent 3,996,064, 1976.
- [7] E. Sum, M. Rychcik, M. Skyllaskazacos, *J. Power Sources* 16 (1985) 85–95.
- [8] E. Sum, M. Skyllaskazacos, *J. Power Sources* 15 (1985) 179–190.
- [9] M. Skyllaskazacos, M. Rychcik, R.G. Robins, A.G. Fane, M.A. Green, *J. Electrochem. Soc.* 133 (1986) 1057–1058.
- [10] M. Skyllas-Kazacos, M. Rychcik, R. Robins, in: AU Patent 575,247, 1986.
- [11] S. Eckroad, Technical Report EPRI-1014836, Electric Power Research Institute, Palo Alto, CA, 2007.
- [12] X.F. Li, H.M. Zhang, Z.S. Mai, H.Z. Zhang, I. Vankelecom, *Energy Environ. Sci.* 4 (2011) 1147–1160.
- [13] S. Kim, J.L. Yan, B. Schwenzer, J.L. Zhang, L.Y. Li, J. Liu, Z.G. Yang, M.A. Hickner, *Electrochim. Commun.* 12 (2010) 1650–1653.
- [14] C.K. Jia, J.G. Liu, C.W. Yan, *J. Power Sources* 195 (2010) 4380–4383.
- [15] T. Sukkar, M. Skyllas-Kazacos, *J. Appl. Electrochem.* 34 (2004) 137–145.
- [16] L. Mou, M. Huang, A. Klassen, M.A.M. Harper, in: WO 2011/050507 A1, 2011.
- [17] W. Wang, S. Kim, B.W. Chen, Z.M. Nie, J.L. Zhang, G.G. Xia, L.Y. Li, Z.G. Yang, *Energy Environ. Sci.* 4 (2011) 4068–4073.
- [18] W. Wang, Z.M. Nie, B.W. Chen, F. Chen, Q.T. Luo, X.L. Wei, G.G. Xia, M. Skyllas-Kazacos, L.Y. Li, Z.G. Yang, *Adv. Energy Mater.* 2 (2012) 487–493.
- [19] L.Y. Li, S. Kim, W. Wang, M. Vijayakumar, Z.M. Nie, B.W. Chen, J.L. Zhang, G.G. Xia, J.Z. Hu, G. Graff, J. Liu, Z.G. Yang, *Adv. Energy Mater.* 1 (2011) 394–400.
- [20] W. Bohnstedt, *J. Power Sources* 59 (1996) 45–50.
- [21] S.C. Chieng, M. Kazacos, M. Skyllaskazacos, *J. Membr. Sci.* 75 (1992) 81–91.
- [22] S.C. Chieng, M. Kazacos, M. Skyllaskazacos, *J. Power Sources* 39 (1992) 11–19.
- [23] T. Mohammadi, M. Skyllaskazacos, *J. Membr. Sci.* 98 (1995) 77–87.
- [24] T. Mohammadi, M. Skyllaskazacos, *J. Membr. Sci.* 107 (1995) 35–45.
- [25] T. Mohammadi, M. Skyllaskazacos, *J. Power Sources* 56 (1995) 91–96.
- [26] T. Mohammadi, M.S. Kazacos, *J. Appl. Electrochem.* 27 (1997) 153–160.
- [27] B. Tian, C.W. Yan, F.H. Wang, *J. Membr. Sci.* 234 (2004) 51–54.
- [28] B. Sun, M. Skyllaskazacos, *Electrochim. Acta* 37 (1992) 1253–1260.
- [29] The flow cell ASR and cycling efficiencies for even the same separator showed small fluctuations. For example, at room temperature, the ASR of Separator C ranges between 1.03 and 1.34 Ω cm², and the EE between 70 and 74% at a current density of 50 mA cm⁻².

- [30] R.A. Assink, *J. Membr. Sci.* 17 (1984) 205–217.
- [31] M. Vijayakumar, M.S. Bhuvaneswari, P. Nachimuthu, B. Schwenzer, S. Kim, Z.G. Yang, J. Liu, G.L. Graff, S. Thevuthasan, J.Z. Hu, *J. Membr. Sci.* 366 (2011) 325–334.
- [32] S.J. Peighambardoust, S. Rowshanzamir, M. Amjadi, *Int. J. Hydrogen Energy* 35 (2010) 9349–9384.
- [33] H.Z. Zhang, H.M. Zhang, X.F. Li, Z.S. Mai, J.L. Zhang, *Energy Environ. Sci.* 4 (2011) 1676–1679.
- [34] H.Z. Zhang, H.M. Zhang, X.F. Li, Z.S. Mai, W.P. Wei, *Energy Environ. Sci.* 5 (2012) 6299–6303.
- [35] S.C. Chiang, Ph.D. thesis, University of New South Wales, Sydney, NSW 2052, Australia.
- [36] F. Rahman, M. Skyllas-Kazacos, *J. Power Sources* 72 (1998) 105–110.
- [37] K. Nath, *Membrane Separation Processes*, Prentice-Hall of India Private Limited, New Delhi, 2008.
- [38] S. Toshio, in: *JP Patent 2815112B2*, 1998.